Photoexcitation and Relaxation Properties of a Spin-Crossover Solid in the Case of a Stable High-Spin State

Cristian Enachescu,[†,‡] François Varret,*[,†] Epiphane Codjovi,[†] Jorge Linarès,[†] Sébastien Floquet,[§] Palanichamy Manikandan,[||] and Periakaruppan T. Manoharan*[,||,⊥]

Laboratoire de Magnétisme et d'Optique, CNRS-Université de Versailles, 78035 Versailles, France, Department of Solid State and Theoretical Physics, Al. I. Cuza University Iasi, 700506 Romania, Institut Lavoisier (IREM), CNRS-Université de Versailles, 78035 Versailles, France, and Department of Chemistry/SAIF, Indian Institute of Technology/Madras, Chennai 600 036, India

Received: July 27, 2005; In Final Form: January 31, 2006

The molecular solid $[Fe^{II}L_2](ClO_4)_2 \cdot CH_3CN$ where L is 2,6-bis(3,5-dimethylpyrazol-1-ylmethyl)pyridine provides a stable high-spin (HS) state at low temperature. Photoexcitation and subsequent relaxation have been studied using light-induced excited state spin trapping [LIESST(H → L)] in the 700−850 nm range, determination of T_{LIESST}, relaxation curves at different temperatures, and temperature dependence of the light-induced spin equilibrium under constant irradiation. The measured photoinduced population of the metastable low-spin (LS) state (<30%) was drastically limited by the concomitant L → H photoprocess. The absence of static light-induced thermal hysteresis and the stretched exponential shape of the relaxation curves respectively revealed the absence of sizable interactions and a large spreading of the activation energies attributed to the ligand flexibility. The whole data set has been simulated using a linear rate equation, with a simplified correction for the bulk extinction of light in the powder sample.

1. Introduction

Thermal and optical switching of spin states[1] is a fascinating game which has already been illustrated by a large number of examples (see ref 2 for most recent reviews). Most of these investigations dealt with spin-crossover compounds, the low-temperature stable state of which is low spin (LS). In such a case, the light-induced properties can be correlated to the shape of the conversion curve, $n_{HS}(T)$. For example, the width of the light-induced thermal hysteresis (LITH)[3,4] was observed to be an increasing function of the width of the thermal hysteresis loop,[5] in agreement with a simple macroscopic model based on a mean-field master equation[6,7] involving self-accelerated relaxation rates.[8−10]

However, similar investigations in the case of a stable high-spin (HS) state have been so far relatively rare.[11−13] This is mainly due to the fact that the accessibility and lifetime of the excited LS state are a priori unknown, since the HS ↔ LS thermal conversion does not occur for entropy reasons. Also, the strength of elastic interactions in the system can be determined only through the relaxation properties. We have performed such an investigation with the molecular solid $[Fe^{II}L_2](ClO_4)_2 \cdot CH_3CN$, where L is 2,6-bis(3,5-dimethylpyrazol-1-ylmethyl)pyridine, here denoted compound **1** which indeed has the stable HS state.[14] It is worth mentioning the flexibility of the L ligand (see Figure 1), the conformational isomerism of which[14] was reported to induce structural transformations[15] in several parent compounds and a distribution of relaxation times[16] in the parent compound (**2**) $[Fe^{II}L'_2](ClO_4)_2 \cdot H_2O$, where L′ = 2,6-bis(pyrazol-1-ylmethyl)pyridine, which has a stable LS state at low temperature.[17]

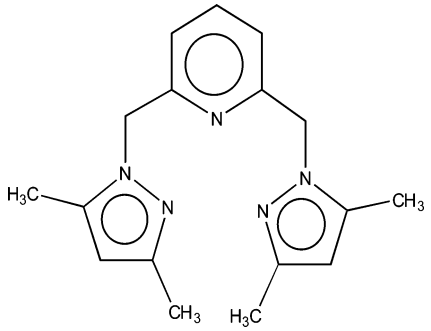

Figure 1. Schematic representation of the tripod ligand, L = 2,6-bis(3,5-dimethylpyrazol-1-ylmethyl)pyridine. Free rotations around the N (pyrazole)−CH_2 and C(pyridine)−CH_2 single bonds are mainly responsible for conformational flexibility.

2. Experimental Section

$[FeL_2](ClO_4)_2 \cdot CH_3CN$ (compound **1**) was synthesized using the procedure developed by Manikandan et al.[14] Elemental analysis performed on the present sample gave the following: C (calcd, 48.77; found, 47.83); H (calcd, 5.12; found, 4.81); N (calcd, 17.38; found, 16.35).

The optical absorption spectrum was determined by reflectance, using a Perkin-Elmer UV/vis/IR Lambda19 spectrometer, through Kubelka−Munk treatment.[18] The magnetic measurements were made using a SQUID magnetometer (Quantum Design MPMS5) operating in the alternative mode, equipped with an optical fiber made of multiwire silica, for light irradiation in the visible-near IR region. The flexible end of

* To whom correspondence should be addressed. E-mail: francois.varret@usq.fr (F.V.); ptm@iitm.ac.in (P.T.M.).
† Laboratoire de Magnétisme et d'Optique, CNRS-Université de Versailles.
‡ Al. I. Cuza University Iasi.
§ Institut Lavoisier (IREM), CNRS-Université de Versailles.
|| Indian Institute of Technology/Madras.
⊥ Honorary Professor, JNCASR, Bangalore and INSA Senior Scientist.

10.1021/jp054149e CCC: $33.50
Published on Web 03/09/2006

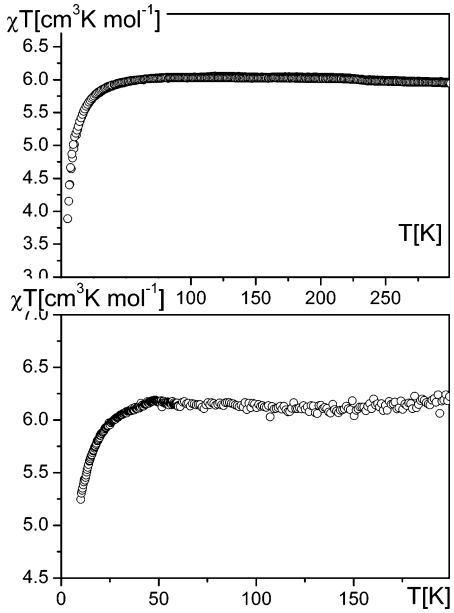

Figure 2. $\chi T(T)$ curves of $[FeL_2](ClO_4)_2 \cdot CH_3C$ from measurements at $H = 1000$ Oe for the bulky sample (top) and the thin sample after photomagnetic holder correction (bottom).

the fiber was connected to a broad-band source of light, with a 100 W tungsten halogen lamp, through 100 nm bandwidth interferential filters, providing intensities up to ~50 mW cm^{-2} in the range 600−800 nm. A very thin sample (~0.5 mg) was needed for photomagnetic measurements, due to bulk absorption and diffusion of light in the powder compound. This sample was inserted between two optical guides, for which a systematic correction was designed, and reported here for the first time (section 2.1). We plotted in Figure 2 the thermal variation of the χT product, measured using a 26.1 mg "bulky" sample in the regular sample holder (top figure) and using the thin sample in the photomagnetic holder (bottom figure) after the correction described in section 2.1. The low-temperature variation is attributed to the zero-field splitting effect in the Fe^{II} HS state.

2.1. Sample Holder Correction. The best photomagnetic sample holder is made of two identical optical guides, made of coated silica, between which a thin sample made of powder compound is stuck thanks to double-sided adhesive tape. Such a sample holder in the SQUID pick-up coils basically behaves as a hole in a continuous diamagnetic matter, that is, adds to the sample data a positive temperature-independent susceptibility term. The latter feature enables doing the sample holder correction in a simple way: the magnetic moment data provided by the bulky sample (mass m_{bulk}) and the thin sample in the sample holder (mass m) respectively are

$$M_{bulk}(H,T) = \chi(H,T) \cdot H \cdot m_{bulk} \quad (1)$$

$$M(H,T) = \chi(H,T) \cdot H \cdot m + \chi_{dia} \cdot H = M_{bulk}(H,T) \cdot m/m_{bulk} + \chi_{dia} \cdot H \quad (2)$$

where $\chi(H,T)$ is the magnetic susceptibility per gram (units of emu g^{-1}) of the compound.

Consequently, the two sets of magnetic moment data obtained in the same field for identical sets of temperatures can be linearly correlated, as shown in Figure 3. The slope of the regression straight line provides the mass ratio, while the shift of the thin sample data provides the sample holder correction, to be systematically applied to all further data. A linear relationship between χT and n_{HS}, the HS fraction, was assumed due to the

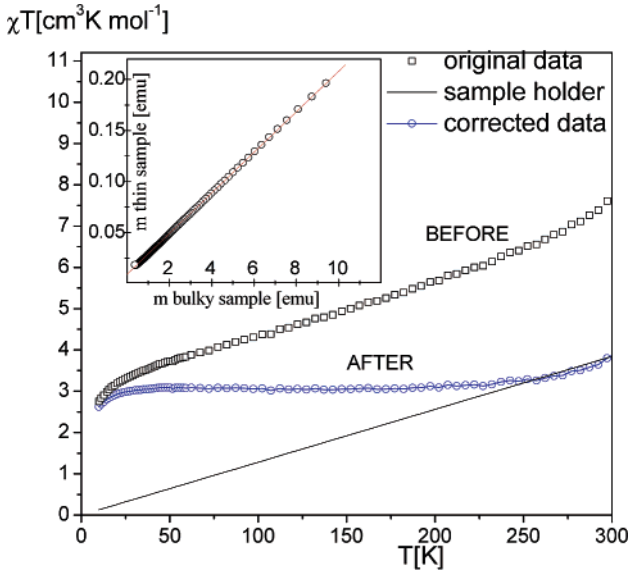

Figure 3. Sample holder correction, from magnetic moment data recorded in the dark at constant field (1000 Oe) and for the same set of temperatures. Inset: the thin sample data in the photomagnetic holder plotted against the bulky sample data. The main figure shows the thermal dependence of χT before and after correction; the straight line stands for the sample holder correction.

weakness of the magnetic interactions between the spin-crossover units. The data were merely normalized, assuming $n_{HS} = 1$ in the stable state, accounting for the (low-temperature) zero-field splitting effect. In addition, small temperature corrections were also systematically applied to the data under permanent irradiation, using Curie law, to account for the thermal heating of the sample (around 2 K at 10 K).[19] Figure 3 also shows an extra increase in the range 250−300 K, which is not reversible and has been attributed to an increase in the sample holder contribution due to viscoelastic lengthening of the plastic straw which housed the silica rods.

3. Results and Discussion

3.1. Mössbauer Spectra. Mössbauer spectra recorded with a fresh sample are shown in Figure 4, with the fitted parameter values listed in Table 1. The large doublet was easily assigned to Fe^{II}(HS), in agreement with the magnetic data. The low-temperature investigation reported here sizably differs from the previous one reported in ref 14. A small second doublet (LS?) was still observed, the relative area of which increased irreversibly, possibly due to solvent removal from the sample kept in a vacuum for long times near room temperature. The conclusion of a basically HS system at all temperatures was therefore obtained, in agreement with the magnetic data presented here for the same sample.

3.2. Light-Induced Excited State Spin Trapping [LIESST-(H → L)] Experiments. We undertook the HS → LS photoconversion [LIESST(H → L)] using suitable wavelengths, which for Fe^{II}(HS) are to be expected in the red edge of the visible spectrum.[20] The spectral absorbance of the powder sample is shown in Figure 5. Absorption bands at 550 and 800 nm are easily assigned to transitions in the LS and HS states, respectively. Their broad character is attributed to the ligand-field distribution associated with the conformational disorder of the ligands. However, the assignment of the third band (~900 nm) was not obvious. Indeed, a spin-forbidden transition of the LS state was reported at ~900 nm in another Fe^{II} compound.[9] However, we observed that irradiation near this wavelength

TABLE 1: Selected Mössbauer Data for $[FeL_2](ClO_4)_2 \cdot CH_3CN$ (Fresh Sample)[a]

order	temperature	sample space	δ_1 (HS) (mm/s)	Δ_1 (HS) (mm/s)	δ_2 (?) (mm/s)	Δ_2 (?) (mm/s)	Γ (mm/s)	area ratio (%)
#1	RT	room	1.055(2)	2.767(3)			0.306(4)	
#5	280 K	vacuum	1.065(2)	3.003(3)	0.50(2)	0.59(3)	0.286(5)	91:9
#4	200 K	vacuum	1.097(2)	3.091(3)	0.54	0.51(5)	0.236(4)	95:5
#3	140 K	vacuum	1.135(1)	3.147(2)	0.58	0.44(8)	0.248(3)	98:2
#2	77 K	helium	1.158(1)	3.167(1)	0.60	0.68(5)	0.250(2)	98:2

[a] Standard notations: respectively isomer shift referred to metallic iron at 300 K, quadrupole splitting and Lorentzian full width at half-height with statistical deviations in brackets. Underlined values were fixed during the fit (for weak lines).

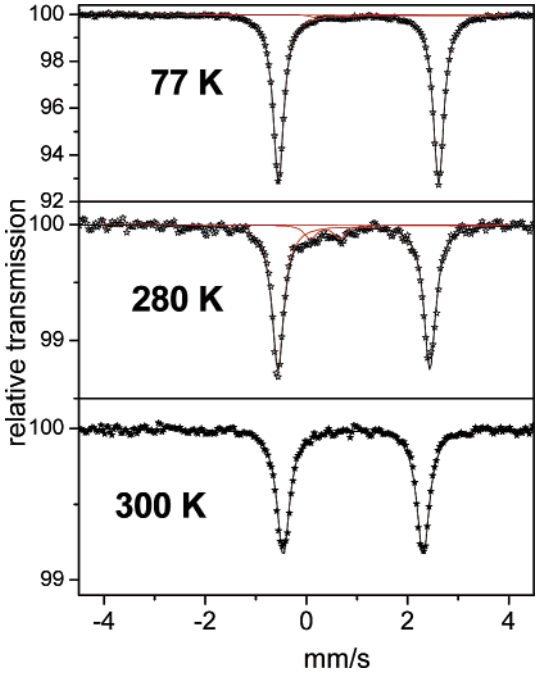

Figure 4. Selected Mössbauer spectra of $[FeL_2](ClO_4)_2 \cdot CH_3CN$ (fresh sample).

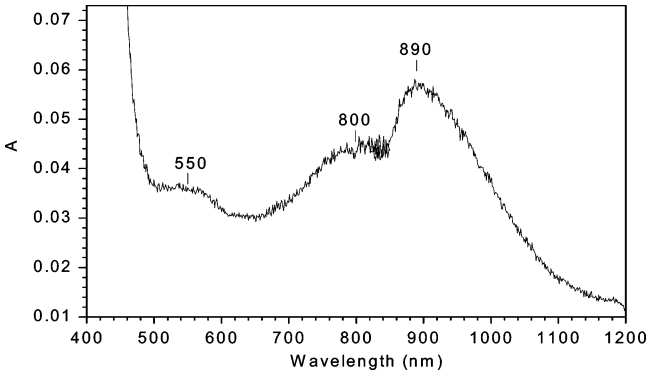

Figure 5. Room-temperature absorbance of pure polycrystalline $[FeL_2](ClO_4)_2 \cdot CH_3CN$.

range (850 nm) did not induce a sizable L → H photoexcitation rate, leading to the conclusion that the third experimental band could not be attributed to the spin-forbidden transition of the LS state. In any case, due to the favorable branching ratio (L → H)/(H → L) ∼ 4:1 reported in Fe^{II} spin-crossover literature,[9] the overlap of the 550 and 800 nm lines, respectively assigned to the LS and HS states, is expected to limit drastically the photopopulation of the LS state.

It appeared from relaxation experiments that the tunneling relaxation could be neglected when analyzing the photoexcitation kinetics at low temperature. It was also anticipated from the following sections that cooperativity is negligible, as it was in the parent compound (**2**).

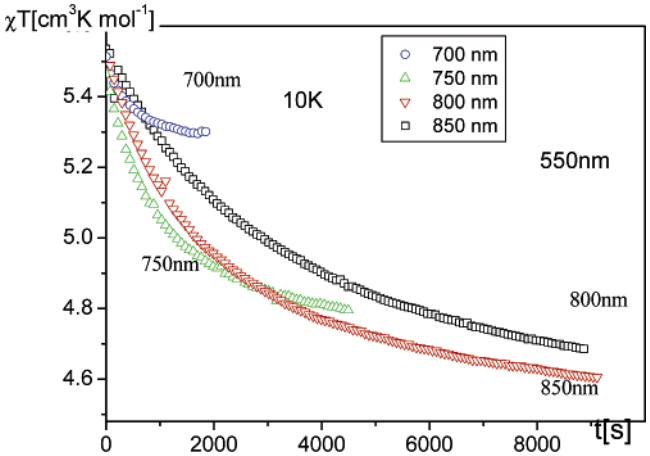

Figure 6. LIESST(H → L) effect of $[FeL_2](ClO_4)_2 \cdot CH_3CN$ at 10 K using different wavelengths. The vertical arrow indicates an efficient reverse LIESST(L → H) using green light.

The model we used is based on the mean-field macroscopic master equation,[6,7] which merely is a single-molecule rate equation. See refs 21−23 for a detailed discussion of the linear approximation suited to noncooperative systems. At low temperature, $k_{HL} \ll k_{LH}$ according to the detailed balance equation ($n_{HS} \gg n_{LS}$ at equilibrium). The linear rate equation is written as

$$\frac{dn_{LS}}{dt} = \eta_{HL} I \sigma_{HL} n_{HS} - \eta_{LH} I \sigma_{LH} n_{LS} - k_{LH} n_{LS} \qquad (3)$$

with $n_{HS} + n_{LS} = 1$ and where $\eta_{HL} I \sigma_{HL}$($\eta_{LH} I \sigma_{LH}$) are transition rates (in s^{-1}) for a HS (LS) molecule to be switched by light to the LS (HS) state, I is the specific intensity of radiation (W cm^{-2}), and $k_{LH}(T)$ is the relaxation rate of the metastable LS state. The temperature dependence of the relaxation rate can be approximated as follows:

$$k_{LH}(T) = k_{LH}^0 + k_{LH}^\infty \exp(-E_A/k_B T) \qquad (4)$$

where k_{LH}^0 is the tunneling rate, E_A the barrier energy, and k_{LH}^∞ the frequency factor of the thermally activated regime, which should be close to the metal−ligand stretching vibration frequencies ($\sim 10^{13}$ s^{-1}).

Using eqs 3 and 4, we made a preliminary fit of the kinetic data, which was reported by dotted line curves in Figure 8. A sizable mismatch could be observed and best displayed by plotting dn_{LS}/dt versus n_{LS} (bottom figure). This kind of plot has been revealed to be useful for investigating the nonlinear characters of the rate equation.[21] Indeed, the linear rate equation (eq 3) leads to a linear plot, with the photostationary value ($dn_{LS}/dt = 0$, e.g., at $t \to \infty$) straightforwardly related to the ratio of the L → H and H → L rates.

In the following, we have modeled the nonlinear behavior evidenced in Figure 8 as an effect of the bulk extinction of light in the sample. The absorption and diffusion processes were

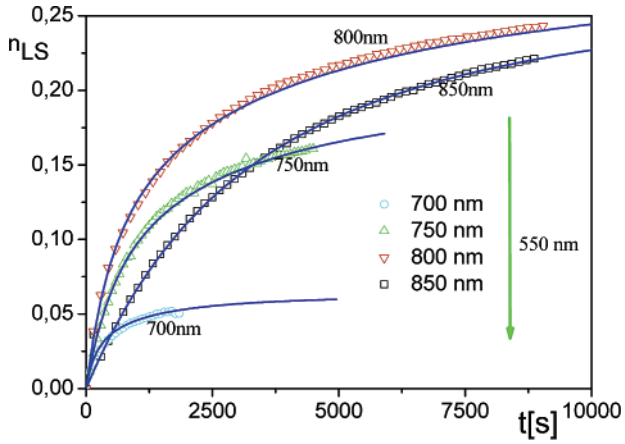

Figure 7. Kinetic curves of the LIESST(H → L) of $[FeL_2](ClO_4)_2 \cdot CH_3CN$ at 10 K, derived from the magnetic data of Figure 6, with best fitted curves (model including intensity decay correction).

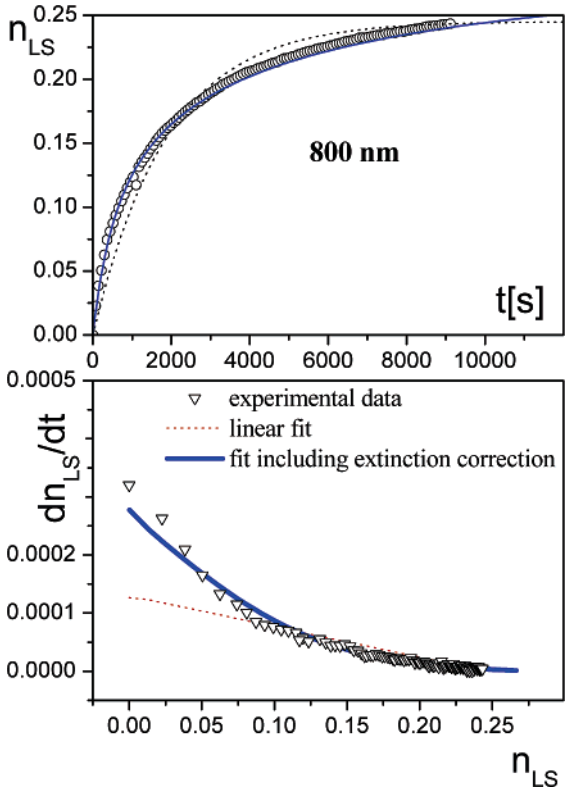

Figure 8. Analysis of the bulk extinction effect, using experimental data from Figure 7, with computed curves neglecting (dotted line) and accounting for (full line) bulk extinction of light.

accounted for by a simple exponential law derived from the Kubelka−Munk solutions[18] to the case of a semi-infinite medium:

$$I(x) = I_0 \exp(-\alpha x) \qquad (5)$$

where x is the depth of the considered layer and α the extinction coefficient (depending on the wavelength). For practical calculations, a single additional parameter, the transmission coefficient $r = \exp(-\alpha X)$, where X is the total depth of the sample, was used, as in refs 16 and 21. The bleaching effect was discarded for simplicity, but this approximation could also be supported because the changes in the spin populations were small (<30%) and consequently were not expected to induce crucial changes of the absorption cross section of the material. Actually, the

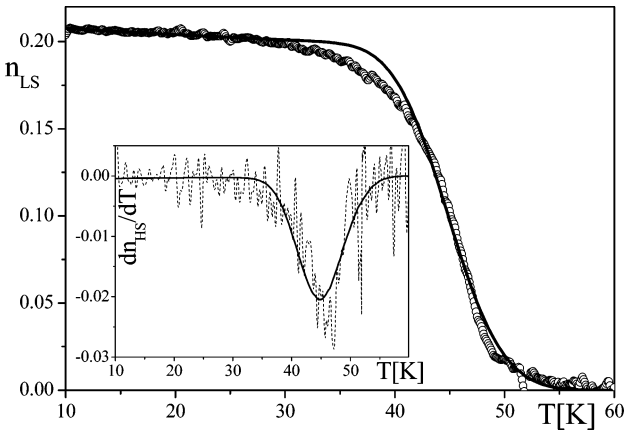

Figure 9. T_{LIESST} curve of $[FeL_2](ClO_4)_2 \cdot CH_3CN$ measured in the dark after photoexcitation: experimental data and the best simulation. Inset: plot of the derivative (dotted line) and computed curve (full line).

TABLE 2: Best Fitted Parameter Values of the Kinetic LIESST Curves of Figure 7

λ (nm)	$I\eta_{HL}\sigma_{HL}$ (s^{-1})	$I\eta_{LH}\sigma_{LH}$ (s^{-1})	$\eta_{HL}\sigma_{HL}/\eta_{LH}\sigma_{LH}$	r
700	0.0003	0.004	0.07	0.14
750	0.0003	0.0011	0.27	0.14
800	0.0004	0.0012	0.33	0.12
850	0.00021	0.00057	0.36	0.10

resulting values of the net transmission factor (see Table 2) of the sample showed a rather weak dependence on the wavelength, in agreement with the optical absorption spectrum, which supported the assumption that the changes in the absorption cross sections of the HS and LS bands finally played a minor role for the extinction properties.

Computed curves with fitted values of the transmission factor, r, have provided a good agreement with the experimental data, as shown by the curves in full lines of Figure 8. Best fitted parameter values are listed in Table 2. The low r values finally support the approximation of a semi-infinite medium. It is also worth noting the complementary characters of the two plots of Figure 8: n_{LS} versus t (top plot) provides accurate information on the photoexcitation rates and their ratio, while dn_{LS}/dt versus n_{LS} (bottom plot) is mainly sensitive to the nonlinear character of the process.

In addition, due to the stretched exponential character of the relaxation curves (see section 3.3), a distribution of barrier energies was introduced, on the example of compound **2**. The system was considered as being made of independent spin-crossover units, each having an activation energy, E_A, with the probability $p(E_A) \approx \exp(-(E_A^{av} - E_A)^2/2\sigma_E^2)$.

3.3. Thermal Activation of Relaxation. We also investigated the thermal activation of relaxation in different ways, either by following the T_{LIESST} procedure[24] after irradiating at 10 K or by following the thermal variation of quasi-static light-induced equilibrium under permanent irradiation.[25] We show in Figure 9 a T_{LIESST} curve, which was obtained in the dark by raising the temperature at the standard scan rate ~0.3 K·min^{-1}. T_{LIESST} is the temperature for which dn_{LS}/dt (or dn_{HS}/dt) peaks, ~47 K here, and denotes the onset of efficient thermal activation of relaxation. A satisfactory agreement with the model was obtained (see Figure 9) by only fitting the kinetic parameters $k_{LH}^0 = 11 \times 10^{-5}$ s^{-1} and $k_{LH}^\infty = 8 \times 10^6$ s^{-1}, while the static parameter values, $E_0 = 1000$ K and $\sigma_E = 80$ K, were taken from the relaxation data reported in the following. The value given here to the tunneling term is only speculative, since it comes from the initial slope of $n_{HS}(T)$, which is very small and

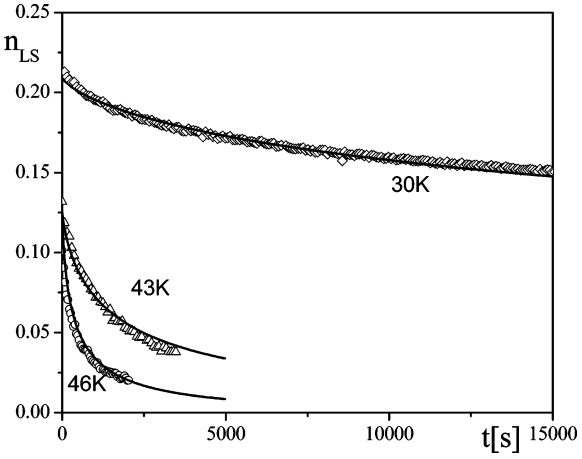

Figure 10. Relaxation curves of $[FeL_2](ClO_4)_2 \cdot CH_3CN$ in the dark.

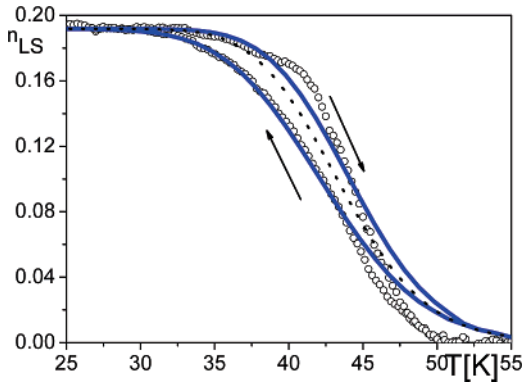

Figure 11. Light-induced thermal hysteresis (LITH) curve of $[FeL_2](ClO_4)_2 \cdot CH_3CN$ at 0.1 K/min and 800 nm. The computed full line accounts for the experimental kinetics. The dotted line stands for the quasi-static limit.

might be crucially affected by the relatively large sample holder correction. Any comparison of the measured T_{LIESST} values to the existing database,[24] which correlates the T_{LIESST} and $T_{1/2}$ values for the *stable LS case*, would be obviously pointless.

In Figure 10, we show relaxation curves measured in the dark at 30, 43, and 46 K. All of them have a typical stretched exponential shape, revealing a large distribution of relaxation times. In the absence of sizable cooperativity, this distribution was assigned to a distribution of activation energies, as for compound **2** (where a larger value of $\sigma_E = 400$ K was used[16]).

3.4. Absence of Light-Induced Thermal Hysteresis (LITH). The thermal evolution of the light-induced spin equilibrium under constant irradiation, for irradiation at 800 nm, is shown in Figure 11. Such an experiment is denoted light-induced thermal hysteresis[3,4] and is sensitive to both the cooperativity of the system[4,5] and the experimental temperature sweeping rate. In the case of a strong cooperativity, the marked self-accelerated character of the relaxation curves induces an instability of the photostationary states,[5,6] giving rise to the so-called quasi-static LITH loop.[4,5]

The computed curve, accounting for the experimental scan rate, is reported in Figure 11. A rather satisfactory agreement was obtained by keeping all parameter values determined so far and merely fitting the intensity factor. It was concluded that the observed hysteresis is purely kinetic in nature. As a matter of fact, the agreement with the experimental data could be slightly improved by introducing a small self-acceleration effect of the relaxation rates, which made the curves a little steeper (the needed cooperative rate equation can be found in refs 4 and 5). However, such a nonlinear effect had to remain small in order to keep the stretched exponential character of the experimental relaxation curves.

The remaining discrepancy in Figure 11, above ~45 K, might also be tentatively assigned to an interplay between the warming and darkening effects of light. Indeed, most spin-crossover compounds undergo (for both L → H and H → L transformations) a bleaching effect during photoexcitation at the appropriate wavelength and conversely a darkening effect, at the same wavelength, during the subsequent relaxation of the metastable state. The darkening effect can be expected to enhance the thermal effect of light in the temperature range where relaxation takes over photoexcitation (say above 45 K in Figure 11) and finally contributes to speed up the thermal relaxation. This possible self-enhancement of the thermal effect of light might specifically contribute to the observed light-induced instability. This effect, to our best knowledge, remains to be specifically investigated in the field of photoswitchable systems.

4. Conclusion

We think we have provided here an example of *complete* investigation of photoexcitation and relaxation properties for the case of the stable HS state. We have concluded that all kinetic effects observed here are consistent with the absence of sizable elastic interactions between the spin-crossover units of compound **1**. A second feature is the stretched exponential character of relaxation, revealing a broad distribution of relaxation times, which we think correlated to the flexible conformation of the ligands, in agreement with the previous study of the parent complex (**2**).

Acknowledgment. P.T.M. thanks the Department of Science and Technology, Government of India, for a research grant (SP/S1/F-18/2000), the INSA, New Delhi, for a Senior Scientist position, and the Indo-French Centre for Advanced Scientific Research (CEFIPRA) for making this collaborative research possible. C.E. thanks the Romanian CEEX Program for a research grant. The Iasi−Versailles collaboration was supported by the European Network of Excellence MAGMANet (FP6-515767-2). The Conseil régional d'Ile de France is acknowledged for supporting the MAGMANEt contract.

References and Notes

(1) Gütlich, P.; Hauser, A.; Spiering, H. *Angew. Chem., Int. Ed. Engl.* **1994**, *33*, 2024.

(2) *Spin-Crossover in Transition Metal Compounds*; Gütlich, P., Goodwin, H., Eds; Topics in Current Chemistry (3 volumes); Springer: Berlin, 2004.

(3) Létard, J. F.; Guionneau, P.; Rabardel, L.; Howard, J. A. K.; Goeta, A. E.; Chasseau, D.; Kahn, O. *Inorg. Chem.* **1998**, *37*, 4432.

(4) Desaix, A.; Roubeau, O.; Jeftic, J.; Haasnoot, J. G.; Boukheddaden, K.; Codjovi, E.; Linarès, J.; Nogues, M.; Varret, F. *Eur. Phys. J. B* **1998**, *6*, 183.

(5) Enachescu, C.; Linarès, J.; Varret, F. *J. Phys.: Condens. Matter* **2001**, *13*, 2481.

(6) Varret, F.; Boukheddaden, K.; Jeftic, J.; Roubeau, O. *Mol. Cryst. Liq. Cryst.* **1999**, *335*, 1273.

(7) Varret, F.; Boukheddaden, K.; Codjovi, E.; Maurin, I.; Tokoro, H.; Ohkoshi, S.; Hashimoto, K. ICMM'04 (Tuskuba, Oct 2004, Japan), *Polyhedron* **2005**, *24*, 2857.

(8) Spiering, H.; Meissner, E.; Köppen, H.; Miller, E. W.; Gutlich, P. *Chem. Phys.* **1982**, *68*, 65.

(9) Hauser, A. *J. Chem. Phys.* **1991**, *94*, 2741.

(10) Jeftic, J.; Hauser, A. *J. Phys. Chem. B* **1997**, *101*, 10262.

(11) Poganiuch, P.; Decurtins, S.; Gütlich, P. *J. Am. Chem. Soc.* **1990**, *112*, 3270.

(12) Hinek, R.; Gütlich, P.; Hauser, A. *Inorg. Chem*. **1994**, *33*, 567.
(13) Hinek, R.; Spiering, H.; Gutlich, P.; Hauser, A. *Chem.—Eur. J.* **1996**, *2*, 1427.
(14) Manikandan, P.; Padmakumar, K.; Justin Thomas, K. R.; Varghese, B.; Onadera, H.; Manoharan, P. T. *Inorg. Chem*. **2001**, *40*, 6930.
(15) Manikandan, P.; Subramoni, M.; Varghese, B.; Manoharan, P. T. *J. Chem. Soc., Dalton Trans.* **1998**, 3219. Manikandan, P.; Muhukumaran, R.; Justin Thomas, K. R.; Varghese, B.; Chandramouli, G. V. R.; Manoharan, P. T. *Inorg. Chem*. **2001**, *40*, 2378.
(16) Enachescu, C.; Linarès, J.; Varret, F.; Boukheddaden, K.; Codjovi, E.; Salunke, S.; Mukherjee, R. *Inorg. Chem.* **2004**, *43*, 4880.
(17) Mahapatra, S.; Mukherjee, R. *Polyhedron* **1993**, *12*, 1603.
(18) Judd, D. B.; Wyszecki, G. *Color in Business, Science and Industry*; Wiley: New York, 1975.
(19) Varret, F.; Noguès, M.; Goujon, A. In *Magnetism: Molecules to Materials*; Miller, J., Drillon, M., Eds.; Wiley-VCH: New York, 2001; Vol. 2, p 257.
(20) Hauser, A. *Chem. Phys. Lett*. **1986**, *124*, 543.
(21) Enachescu, C.; Constant-Machado, H.; Codjovi, E.; Linarès, J.; Boukheddaden, K.; Varret, F. *J. Phys. Chem. Solids* **2001**, *62*, 1409.
(22) Enachescu, C.; Linarès, J.; Codjovi, E.; Boukheddaden, K.; Varret, F. *J. Opt. Adv. Mater*. **2003**, *5*, 261.
(23) Enachescu, C.; Oetliker, U.; Hauser, A. *J. Phys. Chem.* **2002**, *37*, 9540.
(24) Létard, J. F.; Chastanet, G.; Nguyen, O.; Marcen, S.; Marchivie, M.; Guionneau, P.; Chasseau, P. *Monatsch. Chem.* **2003**, *134*, 165.
(25) Boukheddaden, K.; Shteto, I.; Hôo, B.; Varret, F. *Phys. Rev. B* **2000**, *62*, 14806.